

# Statistical analysis of mechanical properties for main cement phases by nanoindentation technique

Jia Fu<sup>1,2\*</sup>, Fabrice Bernard<sup>1</sup>, Siham Kamali-Bernard<sup>1</sup>, Marilyne Cornen<sup>3</sup>

<sup>1</sup> LGCGM, National Institute of Applied Sciences, 35708 Rennes, FRANCE

<sup>2</sup> Material Science and Engineering, Xi'an Shiyou University, 710065, Xi'an, CHINA

<sup>3</sup> UMR CNRS 6226 Institut Sciences Chimique de Rennes/Chimie-métallurgie, INSA de Rennes, 35708, Rennes Cedex 7, France

\* Corresponding author's e-mail: fujia@xsyu.edu.cn

**Abstract.** This work focuses on mechanical properties of some phases of cement-based materials, portlandite (CH), calcite and clinker. Nano-indentation experiment is done on CSM instrument to verify the values of these cement pastes, Young moduli obtained by the averaged experimental load-depth curve is close to other references. The results show that: 1) the Young's modulus of CH averaged by nano-indentation experiment is 39.88GPa, which is in relative good agreement with the 40.30GPa by Constantinides, 36.00GPa by Acker and 45.95GPa by Laugesen. 2) By nano-indentation experiment, elastic moduli of CH, LD C-S-H, HD C-S-H, limestone filler and clinker are separately within the region of 38.8-50.6 GPa, 17.1-27.6GPa, 30.54-36.50 GPa, 79.8-90.6GPa and 94.26-114.18GPa. The elastic moduli are determined by experiment and the SEM image of these phases are verified, which is used to describe the microstructure and mechanical properties of this typical phases in cement paste.

## 1. Introduction

Structural concrete is composed of cementitious composites and concrete performance is related with cementitious composites structural mechanics at different length-scales<sup>[1]</sup>. Portlandite (CH), calcite and clinker are typical constituents of hydrated cementitious of portland cement paste<sup>[2]</sup>, which influences the mechanical properties and the durability of cement paste. Besides, elastic modulus of clinker phases with porosity is reliable, calculated after applying the different porosities on C<sub>3</sub>S, C<sub>2</sub>S, C<sub>3</sub>A and C<sub>4</sub>AF structures<sup>[3]</sup>. As the founding that the elastic properties of the pure phases (C<sub>3</sub>S, C<sub>2</sub>S) and their solid solution alite and belite found in industrial clinker has no obvious difference<sup>[4]</sup>. Young's moduli of CH, calcite and clinker are studied for the modeling of cement at the micro scale<sup>[5]</sup>. Nano-indentation experiment is used to characterize of mechanical behavior at small scale<sup>[6]</sup>, thus to provide the elastic modulus of cement hydration products<sup>[7,8]</sup>.

A large experimental nano-indentation campaign has been led to obtain a data basis of Young's modulus for the various phases of several cement pastes. These results may be used to validate the modeling approaches developed by the authors in previous publications. Although there are some reports on mechanical properties of cement phases, however, these reports basically focus on microstructure or qualitative analysis, and its experimental systematic research on CH, calcite and clinker at nanometers has not yet been studied. Results of nanometer cement phases during nonlinear indentation is used to compare with that of Keinde<sup>[10]</sup> and Constantinides<sup>[11]</sup>. Moreover, elastic



modulus of CH is to compare with that of the Brillouin spectroscopy measurement<sup>[12]</sup>, DFT<sup>[13]</sup> and nano-indentation<sup>[14,15]</sup>. The results of the nano-indentation tests have been already published in reference of Fu et al.<sup>[9]</sup>, this new paper presents the results for pastes with CEM I and Sediments, and with CEM III. Results enable to provide elastic modulus of cement phases for the Multi-Scale Modelling of Computational Concrete platform<sup>[2,5]</sup>.

## 2. Nano-indentation investigation of CH phase at micro-scale

### 2.1. Description of nano-indentation experiment

After the sample preparation and chemical composition, nano-indentation experiment is done on the instrument of INSA de Rennes, the experimental sample and its CSM instrument are in Fig.1.

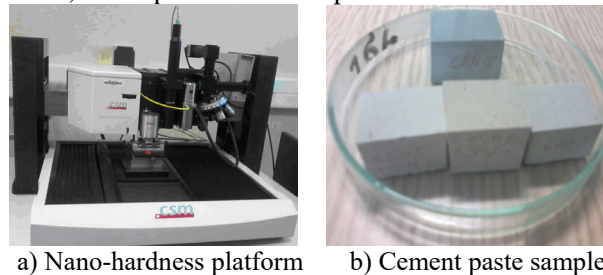


Figure 1. CSM instrument and cement paste used in experiment.

As in Figure 1 a), CSM instruments includes: ultra nano-indentation tester head, nano-indentation tester head, atomic force microscopy and optical video microscope. Samples with the dimension  $1.1\text{cm} \times 1.1\text{cm} \times 1.1\text{cm}$  is in Figure 1 b). Parameters are set to be the same with reference<sup>[9]</sup>.

### 2.2. Chemical composition and sample preparation

Composition and designation of the tested binder pastes are shown in Table 1.

Table 1. Composition and designation of the tested binder pastes

Composition (Kg/m <sup>3</sup> )	B-CEMIII	B-CEMI SD
CEMI	-	303.6
CEMIII	330	-
Limestone filler	240	240
water	210	210
Sediment	-	26.4
water/binder	0.368	0.368

The chemical composition of the cements and mineral admixtures (limestone filler) are in Table 2.

Table 2. Composition and properties of cements and mineral admixtures

Components	CEMIII (%)	CEMI (%)	Limestone filler (%)
CaO	49.9	64.53	-
CaCO <sub>3</sub>	-	-	96.8
SiO <sub>2</sub>	29.1	20.12	0.9
Al <sub>2</sub> O <sub>3</sub>	8.5	5.03	-
Fe <sub>2</sub> O <sub>3</sub>	1	3.12	-
MgO	5	0.98	-
K <sub>2</sub> O	0.32	0.98	-
Na <sub>2</sub> O	0.4	0.16	-
SO <sub>3</sub>	2.67	3.34	-
clinker content (%)	36	98	-
slag content (%)	62	-	-
Specific surface (cm <sup>2</sup> /g)	4263	3649.9	4190

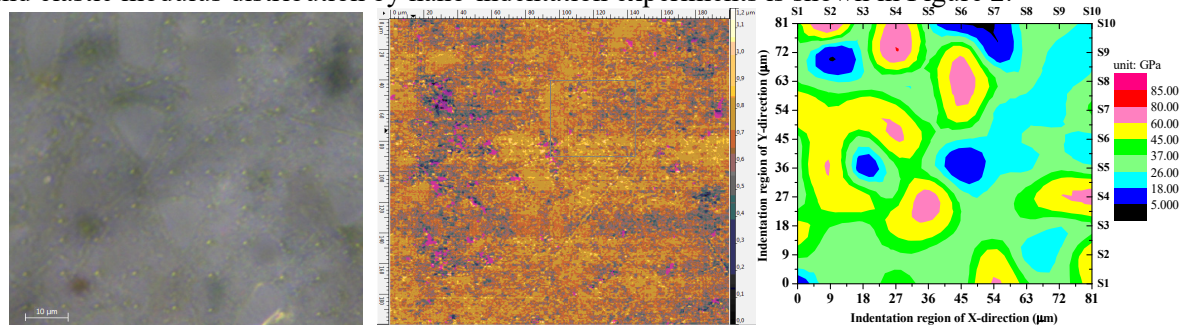
Specific gravity (g/cm <sup>3</sup> )	2.98	3.15	2.7
---------------------------------------	------	------	-----

### 3. Results analysis and discussion

#### 3.1. Regional indentation analysis of B-CEM (III)

Nano-indentation experiment is carried out to determine elastic moduli of cement phases. Bountiful tests is applied to obtain mechanical properties of different phases <sup>[18]</sup>. The reduced modulus is used. For obtaining Young's modulus, the assumption on the value of the Poisson ratio is required to transform from the reduced modulus to Young's modulus, which should be clearly precise.

During data processing of B-CEM(III) sample, we focus on the analysis of hardness range of hydration products, the unhydrated particles will not be considered in statistics. By the order of elastic modulus and hardness from small to large, cement paste ingredients are: a mixture of pores and hydrates, low-density C-S-H gel, high density C-S-H gel and calcium hydroxide, slag hydrates, limestone grains, unhydrated slag particles and unhydrated clinker grains. The value of the Poisson coefficient is set to 0.2. The evolution of the elastic modulus  $E_{HIT}$  (unit: GPa) and maximum depth  $h_{max}$  (unit: nm) as a function of the indented position of the untreated sample are recorded. Typical regional indentation of the B-CEM(III) matrix area (100 indents,  $81 \times 81 \mu m^2$ , indent distance  $9 \mu m$ , force  $1.5 mN$ ) and elastic modulus distribution by nano-indentation experiments is shown in Figure 2.

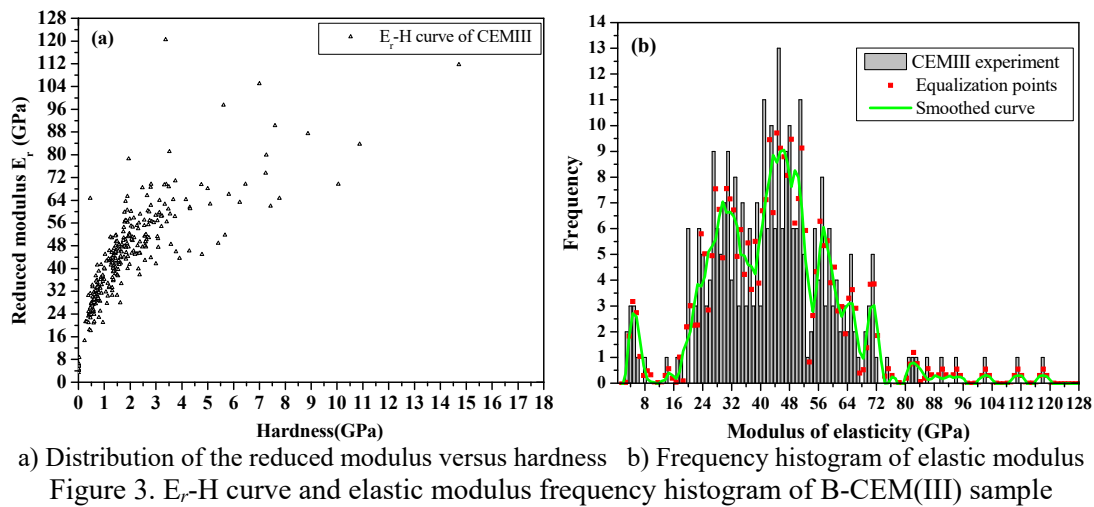


a) Indentation region b) Conscan map of the specimen c) The fitting areas of elastic modulus distribution

Figure 2. Indentation analysis of B-CEM(III) matrix in experiment

Figure 2 a) shows the distribution of  $10 \times 10$  indents performed on the matrix. The marked plane area in Figure 2 b) is about  $50 nm \times 50 nm$ . The indented area is visualized using an optical microscope, whereas the cement matrix region (the distance between two indents is  $9 \mu m$ ) is assigned to the smoothed surface surrounded by the outlined indent area enclosed by the color lines. Figure 2 c) presents the fitting of the contour areas to show the possible surround areas by all data of the indentation points with contrast to Figure 2 a). The real  $E_{HIT}$  distribution of individual indentation points in the indent region to divide the modulus into several ranges. The averaged Young's modulus on the determined 100 indents enable to obtain an approximate mean value of the matrix modulus.

Meanwhile, the mapping matrices and  $E_r$ - $H$  curves according to the experiment data can be used to analyse the main phases in the indentation area. The number of total indents on surface is 363. The  $E_r$ - $H$  curve and elastic modulus distribution by nano-indentation experiments are separately in Figure 3.



As is shown in Figure 3 a), the  $E_r$ - $H$  curve basically turns to a kind of linear relationship. Besides, the averaged elastic modulus  $E_{HIT}$  of all the individual indents is about  $36.695\text{GPa}$  and the averaged maximum depth  $h_{max}$  value is about  $194.57\text{nm}$ . Moreover, we can suppose from Figure 3 b) that elastic moduli of different phases are as follows: LD C-S-H is  $26\text{GPa}$ , HD C-S-H is  $32\text{GPa}$ , CH and slag hydrate (probably stratlingite ...) is  $48\text{GPa}$ , Calcite and slag grains is in the range of  $60\text{--}80\text{GPa}$ .

### 3.2. Regional indentation analysis of B-CEM(I)\_SD

Similarly, during data processing of B-CEM(I)\_SD sample, the Poisson coefficient is set to 0.2. regional indentation of the B-CEM(I)\_SD matrix area ( $144$  indents,  $110\times110\mu\text{m}^2$ , indent distance  $10\mu\text{m}$ , force  $1.5\text{mN}$ ) and elastic modulus distribution by experiments is in Figure 4.

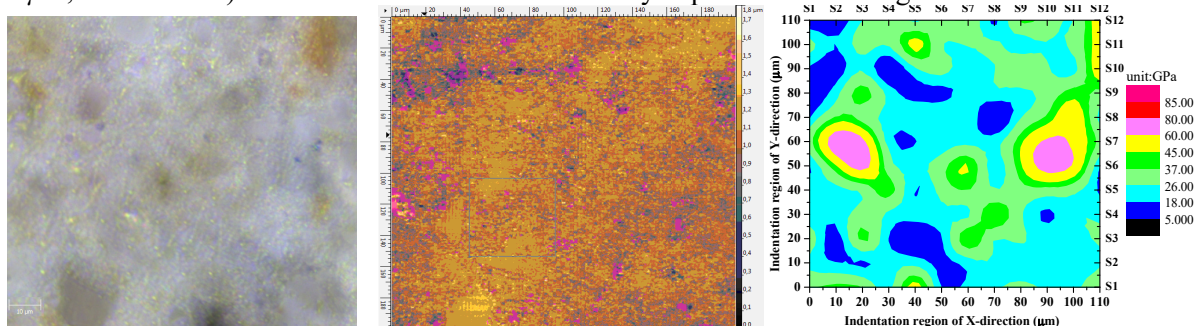
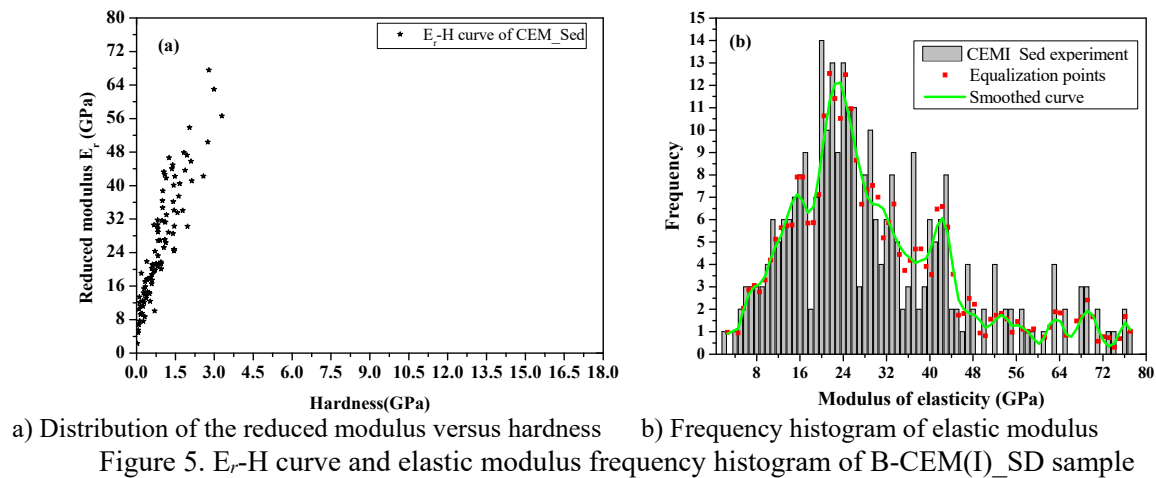


Figure 4. Elastic modulus distribution of B-CEM(I)\_SD by nano-indentation experiments

Figure 4 a) shows the distribution of  $12\times12$  indents performed on the matrix of the B-CEM(I)\_SD sample. The marked plane area in Figure 4 b) is about  $50\text{nm}\times50\text{nm}$ . The cement matrix region (the distance between two indents is  $10\mu\text{m}$ ) is assigned to the smoothed. Figure 4 c) presents the fitting of the contour areas to show the possible surround areas by all data of the indentation points with contrast to Figure 4 a). The indentation hardness  $H_{IT}$  (equivalent to Meyer Hardness and similar to HV for a Vickers indenter) is introduced. The average of Young's moduli on the determined 144 indents enable to obtain an approximate mean value of the matrix modulus.

Meanwhile, the mapping matrices and  $E_r$ - $H$  curves according to the experiment data can be used to analyse the main phases in the indentation area. The number of total indents on surface is 296. The  $E_r$ - $H$  curve and elastic modulus distribution by nano-indentation experiments are in Figure 5.



As is in Figure 5 a), the  $E_r$ - $H$  curve basically turns to a kind of linear relationship. Besides, the averaged elastic modulus  $E_{HIT}$  of all the individual indents is about  $30.08\text{GPa}$  and the averaged maximum depth  $h_{max}$  value is about  $309.20\text{nm}$ . We can suppose from Figure 5 b) that elastic modulus of phases are as: LD C-S-H is  $24\text{GPa}$ , HD C-S-H is  $33\text{GPa}$ , CH is  $43\text{GPa}$ , Calcite is  $60\text{-}76\text{GPa}$ .

### 3.3. XRD spectra results of cement pastes

For various cement pastes, different phases can be determined according to their microstructures. Ye G. et al. [16] have investigated the microstructure of cementitious materials by experiment and simulation. There are different kinds of matrix components in our cement pastes: unhydrated clinker particles and mainly  $\text{C}_2\text{S}$  or  $\text{C}_3\text{S}$ , C-S-H gels (including low density, high density and pouzolanic), CH phase, ettringite phase (needles shape) and other phases (monocarboaluminates, stratlingite and slag etc.). X-ray experiments is proved to be effective, pastes are discussed by Davood [17], in Figure 6.

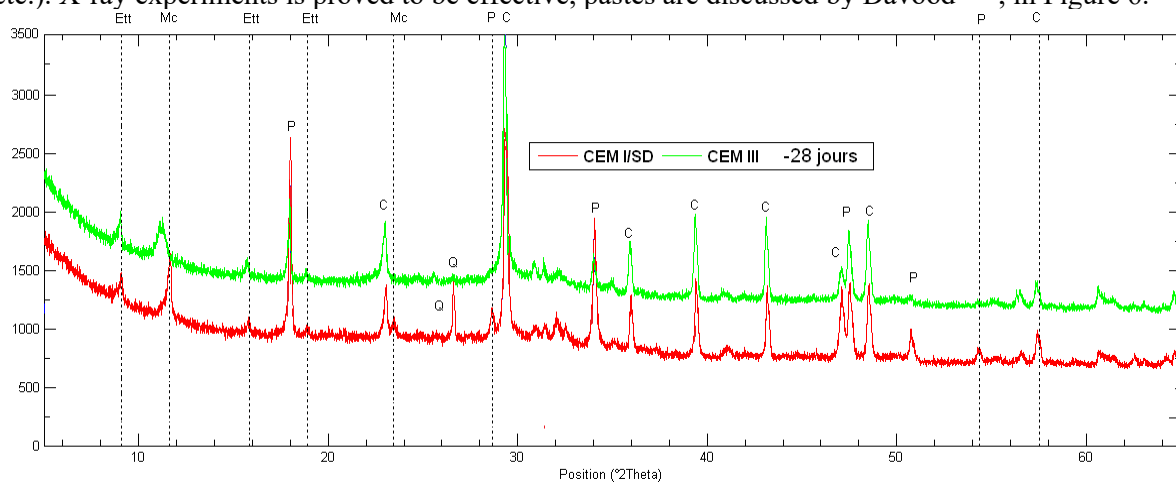
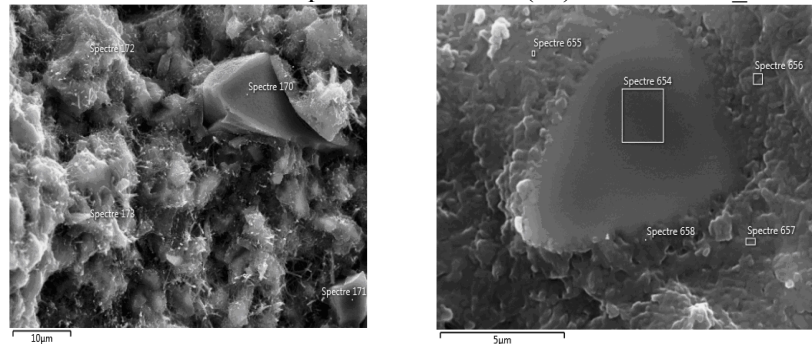


Figure 6 shows the XRD spectra results of different pastes, including B-CEM(III), B-CEM(I)\_SD with an age of 28 days. From Fig.6, the diffraction patterns on samples of binder pastes aged 28 days and 90 days are obtained. It also shows a series of intensive peaks of various substances in the X-ray diffraction curve (the  $2\theta$  angle is  $28.60^\circ$ ). It can be seen that a certain amount of calcite, portlandite, ettringite and monocarboaluminate are presented and characterized in pastes of CEMI\_SD. Besides, the quartz is also detected in CEMI\_SD pastes. Moreover, the peak of portlandite is much less intense for the pastes in which a low content of clinker is also predictable like CEM III paste.



### 3.4. Morphology, composition analysis and microstructure

To highlight the cement phases in samples, SEM analysis are made in university of Rennes 1. Figure 7 shows typical microstructures of different phases in B-CEM (III) and B-CEMI\_SD samples.



a) The test point 170 of slag in B-CEM (III)

b) The Slag of the point 654 in B-CEMI\_SD

Figure 7. Image of typical microstructures in B-CEM (III) and B-CEMI\_SD samples

As can be seen from Figure 7 a), the test points of 170 and 171 are both slag particles with various particle sizes, with a higher elastic modulus in theory. Besides, the test point 173 with the sheet-like structure at the top of the microcrystalline position is possible for C-S-H phase. Meanwhile, in the Figure 7 b), the point 658 correspond to slash hydration product probably stratlingite or slag C-S-H phase and the point 654 corresponds to slag phase.

### 3.5. $E_{HIT}$ frequency histogram of cement phases by nano-indentation experiment

Elastic moduli of LD and HD C-S-H structures by molecular dynamic simulation<sup>[9,18]</sup> and elastic modulus of CH and calcite by density functional theory<sup>[19]</sup> have been investigated in previous studies. However, these phases are not always detectable by simple observation. Then the comparison of  $E_{HIT}$  frequency histogram of samples is drawn, shown in Figure 8.

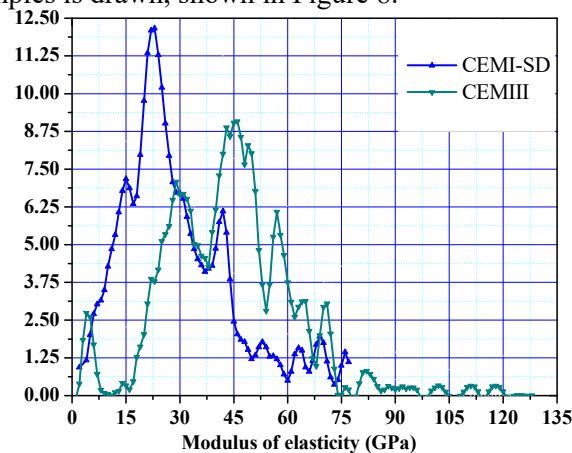


Figure 8 Comparison of  $E_{HIT}$  frequency histogram of two samples

Figure 8 shows comparison of frequency histogram of elastic modulus under various samples. For CH phase, the area of the histogram is within the range of 38.8-50.6 GPa and the averaged Young's modulus is about 40.2-49.2 GPa, which is close to the values of 36.3-44.3 GPa by Constantinides<sup>[10]</sup> and 33.0-39.0 GPa by Acker<sup>[20]</sup>. For LD C-S-H and HD C-S-H phases, the area of the histogram is within the range of 17.1-27.6 GPa (averaged to be 19.65-25.05 GPa) and 30.54-36.50 GPa (averaged to be 29.92-37.12 GPa), which is close to the values of LD C-S-H 14.0-22.4 GPa and HD C-S-H 27.0-32.8 GPa by Constantinides<sup>[10]</sup> as well as to the values of LD C-S-H 18.0-22.0 GPa and HD C-S-H 27.0-35.0 GPa by Acker<sup>[20]</sup>. Furthermore, the latter two peaks which are probably limestone filler and clinker phases, there are some peaks in the range of 60-141 GPa. The ranges of limestone filler and

clinker phases are separately 79.8-90.6GPa and 94.26-114.18GPa, and the averaged Young's modulus are separately  $85.2 \pm 5.3$  GPa and  $104.22 \pm 3.2$  GPa.

#### 4. Conclusion

Nano-indentation experiments are carried out and regional indents are analyzed combined with the observation of morphology and analysis of the  $E_{\text{HIT}}$  frequency histogram. The experimental curves are analyzed and Young moduli are determined by the  $P$ - $h$  curves. Conclusions are as follows:

1) Young's modulus of CH averaged by nano-indentation experiment is 39.88GPa, which is in good agreement with 40.30GPa by Constantinides, 36.00GPa by Acker and 45.95GPa by Laugesen..

2) By nano-indentation experiment, elastic moduli of CH, LD C-S-H, HD C-S-H, limestone filler and clinker are separately within the region of 38.8-50.6 GPa, 17.1-27.6GPa, 30.54-36.50 GPa, 79.8-90.6GPa and 94.26-114.18GPa.

In all, these parameters provide evidence to obtain the mechanical properties of certain cement phases, thus to establish an accurate multi-scale model of concrete on MuMoCC platform.

#### Acknowledgments

The authors acknowledge the financial support provided by China Scholarship Council (CSC). Thanks to Qiufeng WANG for her proofreading. The authors are grateful for the assistance in SEM observations and EDS analysis of the staff of the CMEBA facility (ScanMAT, UMS 2001 CNRS University of Rennes 1) which received a financial support from the Région Bretagne and European Union ( CPER-FEDER 2007-2014)

#### References

- [1] Maekawa K., Ishida T., & Kishi T. (2003) Multi-scale modeling of concrete performance [J]. *Journal of Advanced Concrete Technology*, 1(2): 91-126.
- [2] Kamali-Bernard S, Bernard F., (2009) Effect of tensile cracking on diffusivity of mortar: 3D numerical modelling [J]. *Computational Materials Science*, 47:178–185
- [3] Arar, M. (2016). Elastic properties of cement phases using molecular dynamic simulation.[D] Doctoral Dissertation, Ryerson University.
- [4] Velez K, Maximilien S, Damidot D, et al. (2001) Determination by nanoindentation of elastic modulus and hardness of pure constituents of Portland cement clinker[J]. *Cement and Concrete Research*, 31(4): 555-561.
- [5] Bernard F, Kamali-Bernard S, Prince W., (2008) 3D multi-scale modelling of mechanical behaviour of sound and leached mortar [J]. *Cement and Concrete Research*, 38:449–458
- [6] Vandamme M., Ulm F.J., (2013) Nanoindentation investigation of creep properties of calcium silicate hydrates [J]. *Cement and Concrete Research*, 52: 38-52.
- [7] Ulm F.J., et al.(2007) Statistical indentation techniques for hydrated nanocomposites: concrete, bone, and shale [J]. *Journal of the American Ceramic Society*, 90(9): 2677-2692.
- [8] Sorelli L., Constantinides G. et al., (2008) The nano-mechanical signature of ultra high performance concrete by statistical nanoindentation techniques [J]. *Cement and Concrete Research*, 38(12):1447-1456.
- [9] Jia Fu, Siham Kamali-Bernard, Fabrice Bernard, Marilyne Cornen, (2018) Comparison of mechanical properties of C-S-H and Portlandite between nano-indentation experiments and a modelling approach using various simulation techniques, *Composite part B: Engineering*, 151: 127-138.
- [10] Keinde D. (2014) Etude du béton à l'échelle mesoscopique: simulation numérique et tests de micro-indentation, Doctoral dissertation, INSA de Rennes.
- [11] Constantinides, G.. (2006)Invariant mechanical properties of calcium-silicate-hydrates (CHS) in cement-based materials: instrumented nanoindentation and microporomechanical modeling [D]. Doctoral dissertation, Massachusetts Institute of Technology.

- [12] Speziale S., Reichmann H. J. et al., (2008) Determination of the elastic constants of portlandite by Brillouin spectroscopy [J]. *Cement and Concrete Research*, 38(10):1148–1153.
- [13] Laugesen J.L. (2005) Density functional calculations of elastic properties of portlandite,  $\text{Ca}(\text{OH})_2$  [J]. *Cement and Concrete Research*, 35(2): 199-202.
- [14] Muller Arnaud Charles Albert. (2014) Characterization of porosity & CSH in cement pastes by  $^1\text{H}$  NMR. Thèse de doctorat. École Polytechnique Fédérale de Lausanne.
- [15] Acker P. (2001) Creep, Shrinkage and Durability Mechanics of Concrete and other quasi-brittle Materials, Cambridge, MA, 15-25.
- [16] Ye, G. (2003). Experimental study and numerical simulation of the development of the microstructure and permeability of cementitious materials [D]. Delft University of Technology.
- [17] Davood NIKNEZHAD. (2016). Étude sur les retraites et fissurations de béton autoplaçant à l'état frais et durci : expérimentations et modélisations, Doctoral dissertation, INSA de Rennes.
- [18] Jia Fu, Fabrice Bernard, Siham Kamali-Bernard, (2018) Assessment of the elastic properties of amorphous Calcium Silicates Hydrates (I) and (II) structures by Molecular Dynamics Simulation, *Molecular Simulation*. 44(4):285-299.
- [19] Jia Fu, Fabrice Bernard, Siham Kamali-Bernard, (2017) First-principles calculations of typical anisotropic cubic and hexagonal structures and homogenized moduli estimation based on the Y-parameter: Application to  $\text{CaO}$ ,  $\text{MgO}$ ,  $\text{CH}$  and Calcite  $\text{CaCO}_3$  [J]. *Journal of Physics and Chemistry of Solids*, 101:74-89.
- [20] P. Acker, (2001) Micromechanical analysis of creep and shrinkage mechanisms. In : Ulm, F.-J., Bazant, Z.P., Wittmann, F.H (Eds), Creep, Shrinkage and durability Mechanicns of Concrete and other quasi-brittle Material, Elsevier, Oxford, UK, Cambridge, MA.